Study of scratch resistance of a hard-on-soft polymer bilayer: Combination of in situ vision, X-ray tomography and numerical simulations

Benoît Wittmann, Christian Gauthier, Alain Burr, Jean-François Agassant, Damien Favier, Pierre Montmitonnet, Alain Casoli

Study of scratch resistance of a hard-on-soft polymer bilayer: combination of in situ vision, X-ray tomography and numerical simulations.

Authors: Benoît Wittmann[a,c,*], Christian Gauthier[b], Alain Burr[a], Jean-François Agassant[a], Damien Favier[b], Pierre Montmitonnet[a], Alain Casoli[c]

*Corresponding author. E-mail address: wittmannbenoit@gmail.com

[a] MINES ParisTech, PSL Research University–CEMEF, Centre de Mise en Forme des Matériaux, CNRS UMR7635, Sophia Antipolis, France

[b] Institut Charles Sadron, UPR 22 CNRS, 23 rue du Loess, BP 84047, F-67034 STRASBOURG Cedex 2, France

[c] Tarkett R&D Center, Z.A Salzbaach, L-9559, Wiltz, Luxembourg

Abstract

The deposition of a hard coating is a commonly used solution to increase the scratch resistance of soft polymeric materials at low and moderate normal loads. But the major risk for a coating subjected to tribological stresses is to crack and spall off. In this study, the influence on scratch behavior of a hard polyurethane coating on a plasticized PVC substrate has been investigated. At low load, the hard coating allows decreasing the plastic deformation of the substrate, and a geometrical interpretation is proposed. At increasing loads, this coating shows three fracture mechanisms: first, cracks oriented at 45° to the scratch direction starting near the detachment point behind the tip, on the edge of the scratch ; then, in addition to this first mechanism, tearing under the tip forming a central crack parallel to the scratch direction ; finally, in addition to the first two mechanisms, a circular crack forms ahead of the indentor by a bending effect at the top of the frontal bulge . These mechanisms are observed in situ thanks to a microscope coupled to a camera. Then, the scratches are observed by X-Ray tomography in order to analyze crack propagation in the depth of the material. Finally a numerical model of the scratch test has been developed. The combination of the three techniques gives a precise insight into the local mechanical conditions that lead up to these different kinds of scratches.

Keywords: Scratch test, polymers, coating, tribology, X-Ray tomography, finite elements, damage.

1. Introduction

Protective, anti-scratch coatings are often used on polymeric thin film, e.g. top-coat on paints, varnish on eyeglasses etc. Their anti-scratch performance is strongly connected with their mechanical properties, and their thickness must be optimized with respect to the kind of contact and loading they will be submitted to (1) (2) (3). The scratch test, which has been developed to study resistance of material to tribological agressions, is very often used for coated materials, in particular coated polymers.

During the scratch test of a bulk polymer material, different scenarios can happen. Depending on the material properties and the experimental conditions, five scratch modes are known for uncoated surfaces: reversible (visco)elastic (4) (5) (6), smooth or unstable ductile ploughing (7) (8), folds (9), brittle behavior with cracks in the groove of the scratch (10) (11), machining (7) (12) which corresponds to the degeneracy of a frontal bulge into a chip prone to detach as a wear particle.

Because of the wide variety of observed mechanisms, finding a universal way to increase the scratch resistance of a material is difficult, but a commonly used method in industry is the deposit of an anti-scratch hard coating. This hard coating allows decreasing the plastic deformation of the substrate, hence the residual local slope of the furrow and its visibility. This method works for low to moderate normal loads but leads to complex rupture mechanisms at higher load, making the residual scratch more visible. Indeed, the scratch behavior of a multilayer material depends on the relative mechanical properties of the substrate and the coating. For example, a hard coating on a soft substrate leads to through thickness coating cracking, while a hard coating on a hard substrate leads to chipping (1). Moreover, the scratch behavior of a coated material depends on the adherence between the two layers. In the case of an elastic-brittle coating, when a crack appears in the coating and propagates until the interface, two scenarios can happen: if the adhesion is weak, the crack propagates along the interface and a delamination occurs. If the interface is strong, the crack propagates in the substrate, without delamination (1) (13). In some very particular cases where the substrate and the coating are ductile and the adherence very weak, a stationary delamination regime with a crescent that moves forward ahead of the tip is observed (14) (15).

Because of the numerous parameters having an influence on the mechanical behavior of a material during a scratch test, the interpretation of the mechanisms observed experimentally remains difficult. Thus, numerical models have been developed to study the local mechanical conditions leading to the different mechanisms.

The first numerical simulation of a scratch test by a sharp indenter has been done by Bucaille et al. (16) in 2001 with a conical tip on a bulk material. An elastic – perfectly plastic behavior law (17) has been used. These computations in particular allowed studying the way the material elastically unloads after the passage of the tip, depending on the factor (18):

$$X = \frac{E}{\sigma_0}\cot(\theta) \qquad (1)$$

with E the Young's modulus of the material, σ_0 its yield stress and θ the semi-apical angle of the cone. This X-factor represents the ratio of the average total strain around the indenter ($\cot(\theta)$) to the elastic strain the material may undergo ($\sim\sigma_0/E$). For high X values, the behavior is mainly plastic while for low values, there is an important elastic recovery at the rear face of the tip. Moreover, these first simulations provided a better understanding of the relation between the apparent friction coefficient and the material mechanical properties: for high values of X (dominantly plastic deformation) they

reach the theoretical Goddard and Wilman's value $\mu = \tan(\theta)$ (19) of the apparent friction. However, for lower X values (large elastic strain), the computed apparent friction coefficient is lower than the theoretical value because the sliding is more elastic and therefore the elastic recovery behind the tip is large, decreasing the dissymmetry of the contact shape. Indeed the Goddard and Wilman model has been developed for metals, for which the elastic recovery is negligible compared with their plastic deformation during a scratch test. Finally, an analytical model of friction has been developed, taking into account this elastic recovery (17). Later, they have shown the insufficiency of the elastic – perfectly plastic behavior law by showing that at high penetration depth, the strain hardening of the material has a first order influence on the geometry of the piling-up (8). Another advantage of the numerical simulation is the possibility to study the stresses and strains fields in the material during the scratch. This approach is particularly useful on coated materials to understand the mechanical conditions leading to different complex rupture mechanisms (20) (3) (21) (22) (23) (24) (25) (26). In the case of a thick hard coating on a soft substrate, the coating allows decreasing the plastic deformation of the substrate, which reduces the depth of the residual furrow (23). In the case of a thin coating, the mechanical properties of the coating cannot modify the stress and strain fields of the contact; the thickness of the coating must be adjusted to the roughness of the moving tip to prevent these roughnesses from generating plastic microscopic scratches in the macroscopic furrow left after the contact time (2). Tensile stress behind the indenter causes perpendicular cohesive crack of the coating (22). For scratch test on a soft polypropylene coated by hard polyurethane, H. Jiang et al. (24) have observed that the maximal principal stress moves from ahead to behind the tip with increasing normal load. This is in good adequacy with the rupture mechanisms that they have observed experimentally: in front of the tip at low load, behind the tip at high load. In the same paper, they have compared the scratch resistance of: 1) a soft acrylic coating on a hard steel substrate and 2) a hard polyurethane coating on a soft polypropylene substrate. They observe that, in terms of normal force at which a fracture mechanism is initiated, the hard coating on soft substrate material is better. Demirci et al. (2) have shown for a polymeric hard coating on a softer polymeric substrate that cracking does not appear at the edge of the contact area but under the contact area. Cracking first appears in the rear half of the contact area, whatever the tip velocity and the normal load applied. They described a mechanism of initiation and growing of the cracking recorded in-situ (2). Hamdi et al. (25) studied the mechanical behavior of a bi-layered coating composed of polypropylene (E=1.65 GPa) + Polyamide (E=2.82 GPa) deposited on aluminium (E=70GPa). They compared the scratch resistance of the material depending on the order of the two polymeric layers (aluminum /polypropylene /polyamide and aluminum /polyamide /polypropylene). They concluded that the aluminium / Polyamide / polypropylene is much better because of a lower gradient between the mechanical properties, and a lower friction between the tip and the polypropylene. All these works show the difficulty to analyze the mechanical response and the fracture mechanisms of a layered material during a scratch test because of the high number of parameters and the coupling between some of them, and the difficulty to access experimentally to information on the location of the first damage to understand its mechanism.

Visual aspect is a key problem for the flooring industry. Indeed, the ambience of a room is directly linked to the design of the materials that compose the walls, the ceiling and the floor. In the past, floor covering were made of wood, stone, ceramics or linoleum. But since the second half of the XXth century, PVC based floor covering was developed for performance and economic reasons. Floor covering is daily submitted to various solicitations: walking, sliding chairs, furniture feet indentation, sliding objects, cleaning devices etc. All these solicitations are liable to cause wear of the product and degradation by scratches, which negatively impacts its visual aspect. Therefore, it is protected by a thin layer of a harder polymer.

In this article, the influence of a deposit of hard polyurethane coating on the scratch resistance of a soft plasticized PVC is studied. First, the scratch behavior of an uncoated and a coated PVC are compared. Then, the three rupture mechanisms observed on the coated PVC are analysed in details. The in situ observations of the tip/material contact surface allow observing the place in the surface plane where cracks appear and propagate. The analysis of these mechanisms is completed by a X-Ray tomography observation of the scratch: this complements the 2D visual observations with a 3D view which discloses how cracks have propagated in the depth of the material, without cutting the material with the risk to create new cracks or deform those formed during scratching. Of course one limitation will be the comparison between geometrical information under loading (2D in situ) with those post mortem after unloading (X-Ray tomography). Therefore, a numerical model using the Finite Element Method (FEM) of the scratch test has been developed on Forge NxT to precise the local stress conditions leading to the different rupture mechanisms.

Nomenclature

PVC	Polyvinyl chloride
PU	Polyurethane
E	Young's modulus
ν	Poisson's coefficient
σ_y	Yield stress
m	Strain hardenning coefficient
T	Temperature
μ	Coulomb's friction coefficient
R	Radius of the tip
a_c	Contact radius
d	Indentation depth
ε_{eq}	Equivalent deformation
P_{pl}	Plastic dissipation power
$\overline{\sigma}_{eq}$	Equivalent stress
$\dot{\bar{\varepsilon}}_{pl}$	Equivalente plastic strain rate
$t_{coating}$	Coating thickness
S_a	Roughness arithmetical mean height

2. Materials and methods

2.1. Microvisio-Scratch

As described in (4), the apparatus is a homemade set-up based on a commercial servomechanism allowing the scratching action by moving the sample relative to the tip. The scratch test can be piloted in normal force (from 0.05N to 35N) and in scratching velocity (from 1 to 10^4 µm/s). Moreover, the sample is enclosed in an insulated box allowing a control of the temperature (from -50°C to 110°C) and moisture. A microscope coupled to a camera allows an in situ vision of the contact area provided transparent samples are used. A detailed diagram of the apparatus and an example of a scratch test performed on a perfectly transparent sample are in appendix A. Since the camera is located at the same abscissa as the indenter, its optical axis is normal to the interface; furthermore, the two materials have very close indices of refraction. Hence the interface does not degrade the transmission of light.

A first scratch is done on uncoated PVC, and a second one on coated PVC. Both are performed in the same conditions: T = 22°C, ambient humidity, with a spherical tip of radius R = 100 µm. The velocity is constant at 30 µm/s. The tests are done in 10 increasing normal force steps, from 0.2 N to 3 N.

All the tests have been doubled to check repeatability. The latter has been found very good in all cases.

In the following of this article, all lengths will be normalized by the tip radius R.

2.2. Samples studied

The first sample is a flexible plasticized PVC sheet (thickness = 6 R). The second sample is composed by the first sample covered by a hard filled polyurethane anti-scratch coating (thickness $t_{coating}$ = 0.2 R). The role of fillers is not to increase the scratch resistance of the material, but to control its gloss. The uncoated PVC has a roughness S_a = 180 nm and the coated one has a roughness S_a = 712 nm. S_a is the arithmetical mean height, defined as :

$$S_a = \frac{1}{L^2} \int_0^L \int_0^L |z(x,y)| \, dxdy \qquad (2)$$

With x, y and z the spatial coordinates of the topography of the sample. Altitude z is referred to the mean plane and L is the sampling length.

The mechanical properties of each material have been measured by tensile tests on an Instron 3344 (Instron, Norwood, USA) at 22°C and a deformation rate of 0.3 s^{-1}. Three tensile tests were performed on each material. In tension, the PVC has an elastic-plastic behavior and the PU has an elastic-brittle behavior. The mechanical properties of both materials are given in the table 1. They are rendered non-dimensional using the Young's Modulus of the PVC.

	PVC	**PU**
Non- dimensional E	1 (± 0.06)	6.7 (± 0.5)
ν	0.3	0.4
Non dimensional σ_y	0.027 (± 0.00033)	N/A

Table 1: Mechanical properties of the materials. The Young's modulus and the yield stress are normalized by the Young's modulus of the PVC. The PU has no yield stress because it has an elastic-brittle behavior. Poisson's coefficients have not been measured but taken from literature.

2.3. Tomography

The characterization of the scratched samples has been performed by a X-Ray Solution tomograph, model Easytom 150-160 (RX solution SAS, Chavanod, France). The X-Ray generator is an open tube Hamatsu Microfocus with a tungsten filament and a tungsten target. The detector is a matrix plane sensor ("Flat Panel") Varian PaxScan 2520DX 1920x1536 pixels (pixel size = 127 µm x 127 µm) – 16 bits. The scan is done with the following parameters: Resolution = 1.2 µm, Source – sample distance = 3.29 mm, source – sensor = 347 mm, X-Ray energy = 80 kV, beam intensity = 65 µA. 1984 projections are done over 360°. Averaging = 15 images per position. The sensor has a cadence of 2 images per second. The whole scan lasts 4.5 hours. The reconstruction method used is the filtered back projection.

2.4. Confocal microscopy

The roughness of the samples and the depth of the residual grooves has been measured by a STIL confocal microscope (STIL SAS, Aix-en-Provence, France), with a MG140 optical pen (-x,-y

resolution = 2µm; -z resolution = 30 nm; maximum light cone angle = 27°). The samples are positioned on a x-y stage, measurements have been carried out with x and y steps of 5 µm.

2.5. Numerical model

The numerical model of the scratch test has been set up in the commercial implicit (quasi-static) FEM software Forge NxT (version 3.0) in view of its remeshing capacity and the large mesh distorsions observed. As shown figure 1, the tip is modelled by a spherical analytic rigid solid of radius R. The material is defined as a parallelepiped (20 R x 6.2 R x 5 R). This parallelepiped is defined as a multiple material object: Instead of defining one object for the PVC, another object for the PU, and defining a contact law between the two, only one domain is defined with a unique mesh in which two zones are defined: a first one below the plane z = 6 R, and a second above this plane. The behavior law associated to each finite element depends on its position compared to this plane: the PVC constitutive model is used for elements below and the PU model for elements above. As shown figure 1, there is no element crossing the interface, which would increase incertitude and numerical noise. This approach is less time consuming than the multi-domain approach because there is no contact to compute between the two materials. Note that the initial meshing as well as remeshing strategies allow a well-defined, plane, smooth interface (see fig 1). The main limitation of this single domain strategy is that it does not allow delamination and conclusions will be restrained to systems with high interface adhesion. This is not a detrimental limitation for the experimental material studied (PVC / PU), because it has been observed experimentally that the adherence between the PVC and the PU is sufficient to avoid delamination even under the most severe loadings applied in this work (see part 3.1.3).

The plane y = 0 is a symmetry plane. The planes x = 0, x = 20 R and y = 5 R are defined as symmetry planes too in order to prevent any perpendicular displacement. The stresses computed close to these borders are found negligible compared with the stress around the tip ; this allows concluding that the domain considered is large enough to avoid edge effects.

The software uses four node tetrahedra which allows automatic, unstructured remeshing, with a $P1^+$-P1 stabilized formulation. Here, remeshing is forced in the whole domain every 10^{th} time increments (time increment $\approx 3.8.10^{-3}$s). The nodes on the PVC/PU interface are fixed in order to keep a well-defined interface throughout the computation.

Far from the tip, the mesh is coarse (0.5 R). Just under the interface, in the PVC, the mesh in finer (0.1 R) on a width of 1.5 R along the Oy axe. In the PU zone, the mesh in very fine (0.03 R) on a width of 1.5 R along the Oy axe.

The PU is modeled by an isotropic linear elastic law with $E_{PU} = 6.7$ (normalized by the young modulus of the PVC) and $\nu_{PU} = 0.4$. The PVC follows an elasto-plastic law: $E_{PVC} = 1$ (normalized by the young modulus of the PVC), $\nu_{PVC} = 0.3$ and the stress - plastic strain curve is given by the power law:

$$\sigma = A\,(\varepsilon+\varepsilon_0)^m \qquad (3)$$

with A = 0.054 (Unitless because normalized by the Young's modulus of the PVC), m = 1.80, and $\varepsilon_0 = 0.68$.

Friction is modeled by a Coulomb law with $\mu = 0.35$. It is the value of the apparent friction that is measured experimentally at low load, when the obstacle component of the apparent friction coefficient is negligible compared with the local friction component (27).

The rupture of the material is not modeled because the objective of these computations is only to determine the stress fields leading to the different fracture mechanisms.

In sections 3.2.1 and 3.2.2, the test is piloted by normal force imposed to the tip. In section 3.2.3, a vertical displacement is imposed to the tip and the normal force is computed. The material moves in the –x direction on a length of 10 R which has been checked systematically to be sufficient to reach a steady state, as in the experiments.

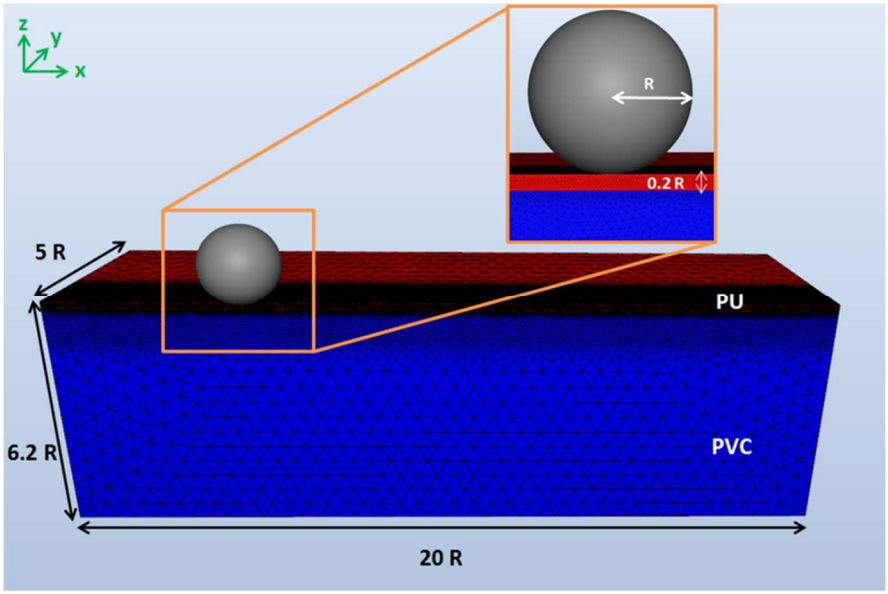

Figure 1: Numerical model of the scratch test

About the computation done on uncoated PVC, the same model is used with only one difference: the material is not defined as a bi-material object and the PVC behavior law is used everywhere.

3. Results

3.1 Experimental results

3.1.1 Deformation and rupture modes observed

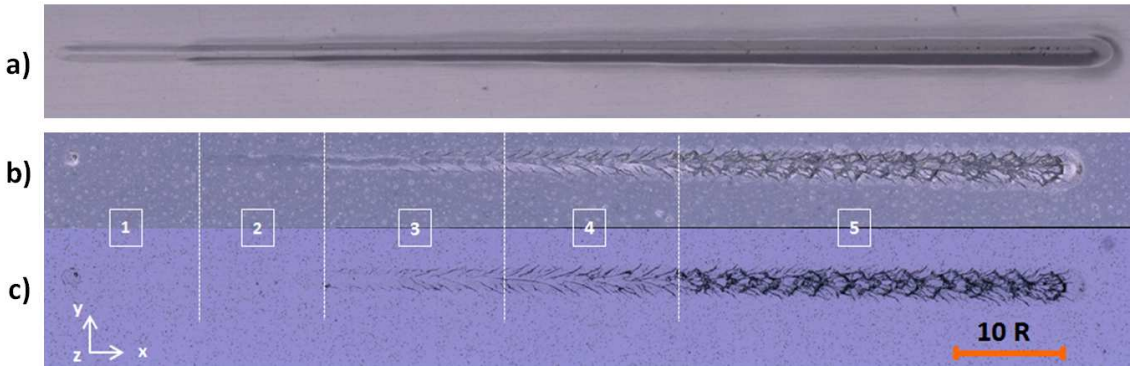

Figure 2: Photographs of the residual scratches. Scratch done on uncoated PVC (a). Scratch done on coated PVC, observed in reflection (b). The same scratch on coated PVC, observed in transmission (c). The reflection lightening allows a good visualization of the local slopes (lateral and frontal bulges are clearly visible, lighter grey) and the transmission lightening allows a better visualization of cracks. The combination of both allows a good visualization of the 5 types of behavior respectively: 1) elastic sliding, 2) elastic plastic scratching, 3) 1st fracture mechanism, 4) 1st and 2nd fracture mechanisms, 5) 3 kinds of fracture mechanism simultaneous.

Figure 2a is a photograph of the residual scratch performed on uncoated PVC. This scratch test has been performed two times, with exactly the same results : there is a ductile groove and no cracks: the material is deformed elastically and plastically during the whole test.

The corresponding photographs of the residual scratch on PVC coated by polyurethane (figures 2.b and 2.c) show five distinct areas at increasing normal force. Again, this scratch test has been performed twice and the different mechanisms appear at the same normal load for the two tests.

Thanks to a microscope coupled to a camera, the contact area between the tip and the material is observed in situ i.e. continuously during the test, showing the very moments and locations at which cracks appear. Figure 3 shows an in situ photograph for the main steps of the scratch shown on figure 2.c. Since it is difficult to determine precisely the contact area from only one photograph, its evaluation is helped by the video. Indeed, the movement given by the video offers a better vision of the contact. There is, in the supplementary material of this article, an animated figure showing a part of the video for each step, allowing a better visualization of the phenomena.

1: The material is deformed almost exclusively elastically. The contact area is circular and there is no residual groove after the contact time.

2: The substrate is deformed plastically and the contact area is not circular anymore. The material does not totally recover behind the tip because of plastic yielding, so that a residual groove is observed on the post-test photograph.

3: Cracks appear on the rear edge of the contact, oriented at ~ 45° to the scratch direction Ox, pointing towards +x. The intercrack distance is rather regular (≈ 1 contact length).

4: In addition to the cracks at 45°, still visible, the coating tears under the tip. It first opens parallel to the scratch direction and propagates in the direction Ox, following the movement of the tip. After a

propagation of few contact lengths, the crack deviates towards the side of the groove; then another one appears under the tip, generally deviating later towards the other side of the scratch in a rather regular manner. The intercrack distance is rather regular as well (≈ 2 contact length).

5: In addition to the cracks at 45° and the tearing under the tip, a circular crack appears beyond the front edge of the contact, perpendicularly to the tip, periodically also, every one or two contact lengths.

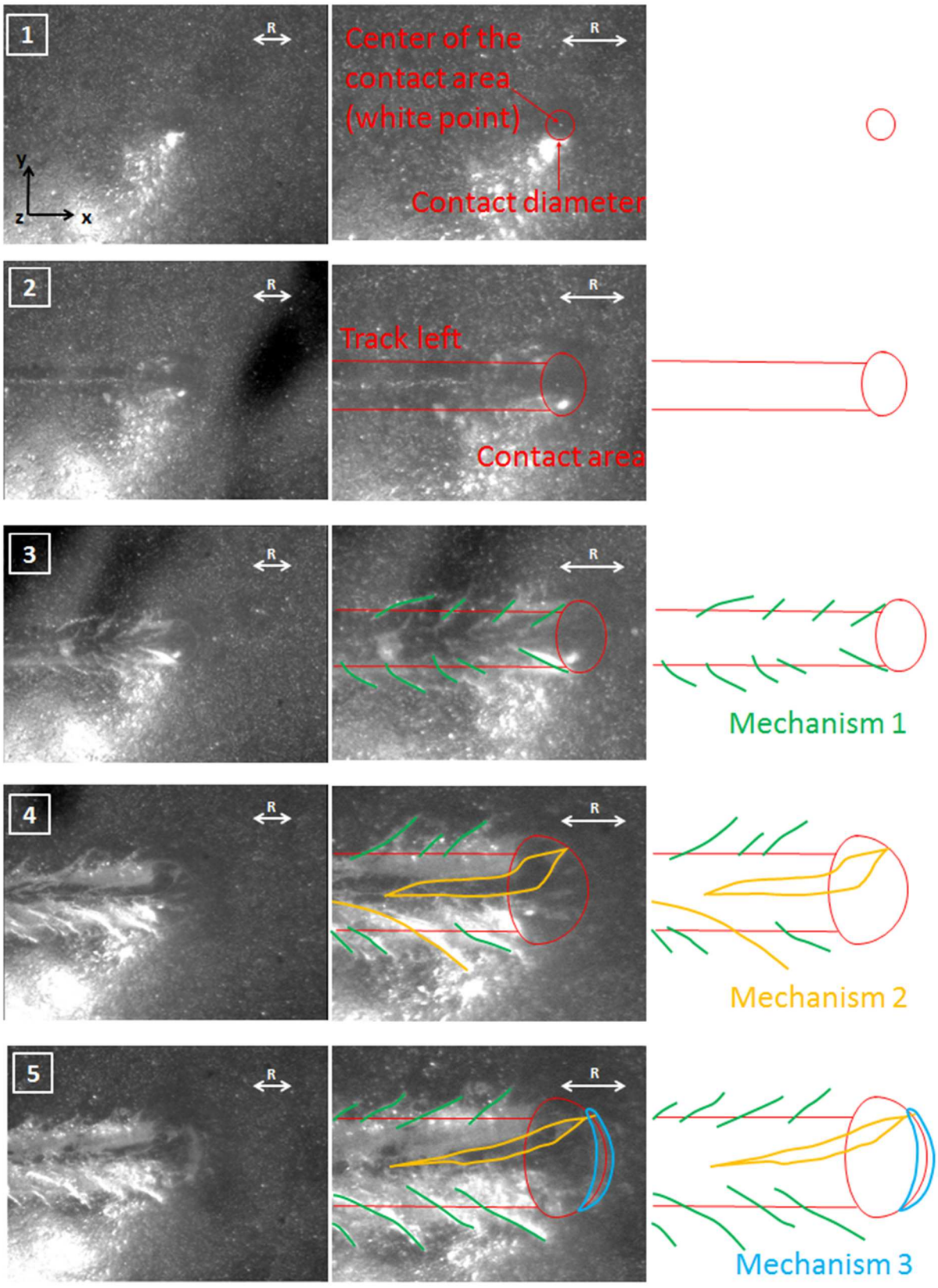

Figure 3: In situ photographs and schematic representation of the damage regimes. Photograph numbering corresponds with the text. An animated version of this figure is in the supplementary material of this article, allowing a better visualisation of the different mechanisms.

3.1.2 Depth of the residual grooves

The roughness has been measured along the scratches done on uncoated and coated PVC in order to compare the residual grooves. The measurements, performed by confocal profilometry, are shown in figure 4.

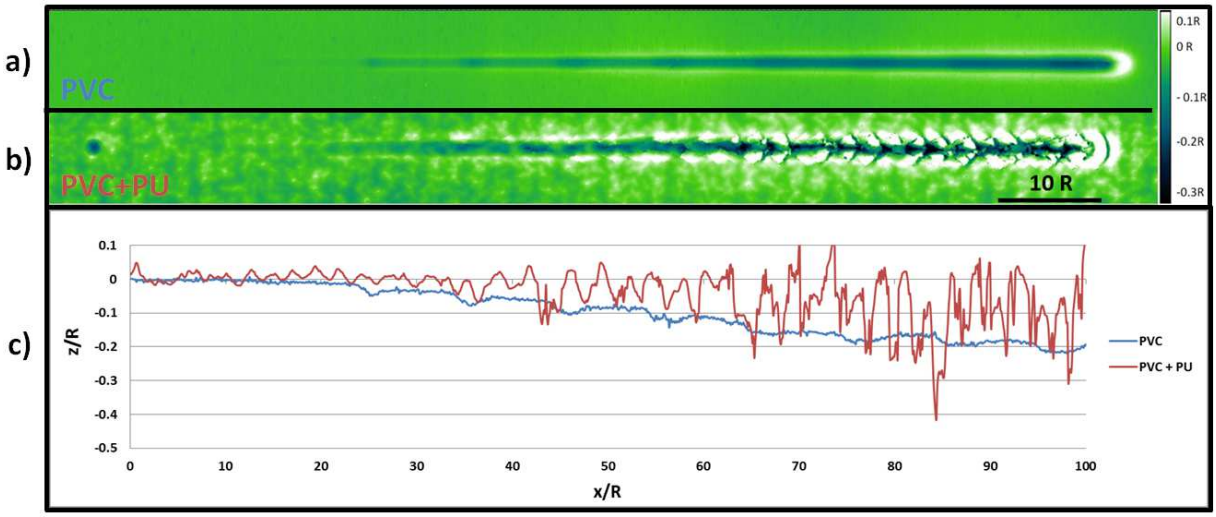

Figure 4: Depth of the residual grooves: on uncoated PVC (a), on coated PVC (b). Comparaison of the profiles of the bottom of the groove in the (xz) vertical-longitudinal plane, uncoated and coated PVC (c)

From x/R = 0 to 10, there is almost no influence of the coating on the mechanical response of the material: on coated as well as uncoated PVC, there is no residual depth meaning that the material deformed almost totally elastically; the coated sample is rougher due to the filler, the size of which is not small compared with the coating thickness. From x/R = 10 to 60, the residual depth on coated PVC is clearly lower than on uncoated PVC. This means that uncoated PVC deforms plastically whereas elasticity is more pregnant on coated PVC; whether this effect is mostly due to the depth under load being smaller (protection of the soft substrate by the hard coating) or to elastic recovery after unloading being larger, cannot be told at this stage. From x/R = 60 to 100, the residual depth is again lower on coated PVC, in average, but the profile is very rough along the groove, because of the fractures that happen at this load level.

It can be concluded that profilometry captures the cracks morphology to a certain extent. The highest points are measured well above the initial surface level, which means that rotation of fractured blocks of PU has occurred beyond x/R = 60. It is not possible at this stage to tell if the lowest points are on the interface. Tomography is therefore used to describe the cracks with more precision.

3.1.3 Tomography characterization

In situ observation gives a lot of information leading to a better understanding of the mechanisms involved. However, it only gives information in the (xy) plane, as illustrated in figure 3, it does not give any information in the plane (yz) perpendicular to the plane of the surface. One possibility could be to cut the material after the test in order to study the cracks propagation in the depth in the plane (yz). This method is risky because new cracks could be created by cutting and wrongly attributed to the scratch test. In order to avoid this problem, the scratch is analyzed nondestructively by X-Ray tomography. This tomography, reported figure 5, has been performed on part 5 of the scratch of figure 2, where all three types of cracks are present.

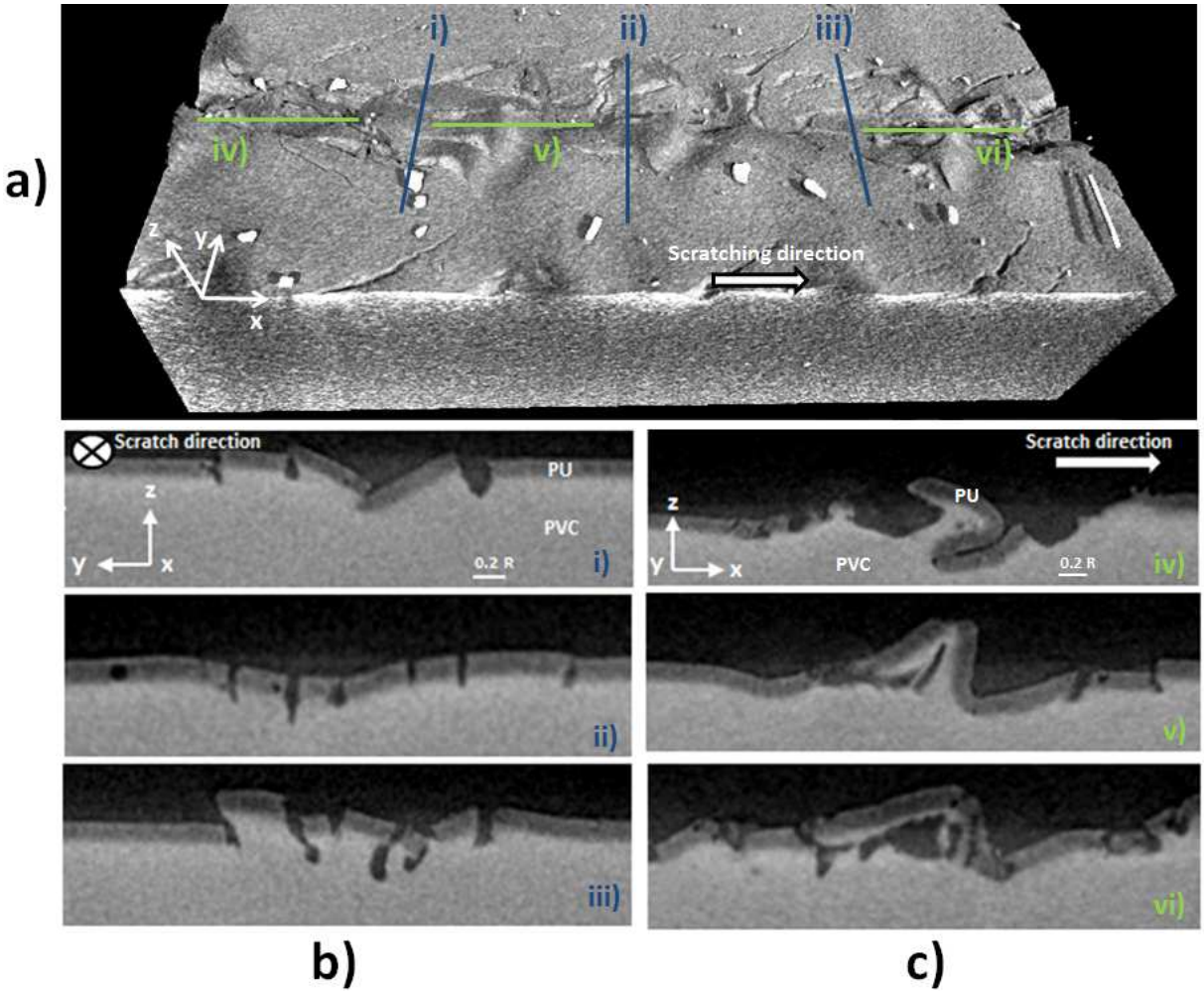

Figure 5: Tomography of the scratch of figure 2 (part 5). 3D Representation (a), 3 cross sections in (yz) planes for different x positions (b), 3 cross sections in (xz) planes for different x positions (c). The lines i) to vi) show the locations of the cross sections.

The cross sections in the (yz) planes (figure 5.b) show that there is no delamination between the two layers, although it is evident that very severe deformation has taken place. This has been found systematically. Some cracks that initiated in the PU have propagated into the PVC. Cracks never propagate along the interface, but always in the PVC, which testifies for a good adhesion between the two layers. This legitimates for this particular system the hypothesis of ideal adhesion done in the numerical model.

Another tomography measurement was done on the whole residual scratch, in order to distinguish the different steps and analyse separately the different rupture modes. The results are in appendix B.

First, this tomography shows that the first mechanism only concerns the coating, it doesn't propagate in the substrate. Then, the second mechanism concerns the coating and the substrate. Indeed, this mechanism is visible until a depth of $\approx 0.35R$. Finally, the last mechanism concerns the coating and the substrate, as it is observed until a depth of $\approx 0.4R$.

Furthemore, the visualisations in the planes (xy) and (yz) well show that the 3 mechanisms superimpose to each other with increasing force, without disrupting each other.

3.1.4 Influence of the fillers on the mechanical response

A scratch test was perfomed on the PVC covered by 0.2R of PU without filler in order to observe the influence of the roughness on friction, and the influence of the fillers on crack initiations. This coating has a roughness S_a = 96 nm. The scratch test has been performed under exactly the same conditions as the one presented figure 2.c. This experiment has been done two times, the repeatability is fair and a representative photograph of a residual scratch is shown figure 6.

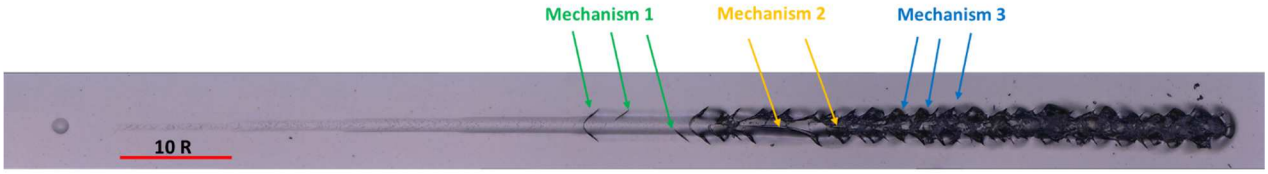

Figure 6 : Photograph of the residual scratch done on PVC coated with unfilled PU

The three same mechanisms appear with filled and unfilled coating. There is in the supplementary material of this article an animated figure showing in situ videos of the apparition of each mechanism. However, we note two main differences in the two tests :

1) The local friction is different : μ = 0.35 with filled PU and μ = 0.7 with unfilled PU (The local friction is measured in the beginning of the test, for F_n = 0.2N.
2) The occurrence of the 3 mechanisms is less regular. With filled PU, the mechanisms 1 and 2 appear regularly and periodically. With unfilled PU, the mechanisms appear irregularly, there is a general periodicity but some occurrences are missing. On figure 6, it is very clear for the mechanism 1. An explanation is proposed paragraph 4.7.

3.2 Numerical simulations results

3.2.1. Validation of the model

A numerical simulation of each scratch (on uncoated and coated PVC) has been carried out with a normal load of 0.5N, which corresponds to the second part of figure 2 (ductile deformation for uncoated and coated material). The first objective is to compare the numerical results to the experimental ones, in order to validate the model. Figure 7 shows the comparison of the modeled and the experimental contact areas between the tip and the material, on uncoated and coated PVC.

- Uncoated PVC: a_c/R = 0.82 in the experiment and a_c = 0.65 in the model. The order of magnitude are consistent, even if the PVC is a little bit more rigid in the model. Moreover, there is a large ductile groove behind the tip. This large groove is also present in the numerical model.
- Coated PVC: a_c/R = 0.49 in the model and a_c = 0.4 in the experiment. Again, the order of magnitude are consistent, even if the material is a little bit more rigid in the model. Moreover, the ductile groove on the coated material is much smaller than on the uncoated one, for both numerical model and experiment.

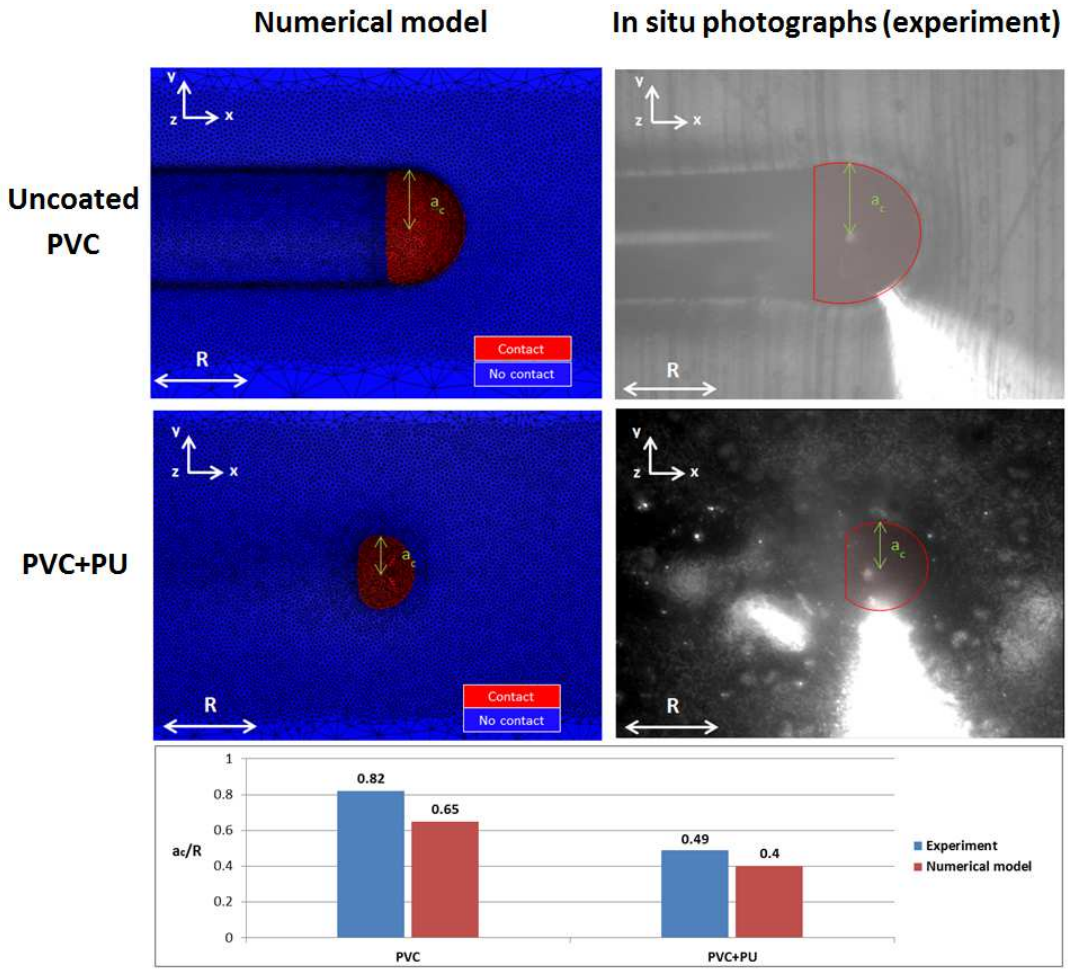

Figure 6: Comparison of the contact radius between the experiment and the numerical model for a normal load of 0.5N on uncoated PVC (above) and on coated PVC (in the middle). The graph (below) summarizes the four values of a_c

3.2.2 Comparison between coated and uncoated material

From the same two computations than the ones presented in part 3.2.1, we are interested in the contact geometry between the tip and the material, in the plane (yz), during the contact and after elastic unloading. The results are shown figure 8 as cross sections of the grooves.

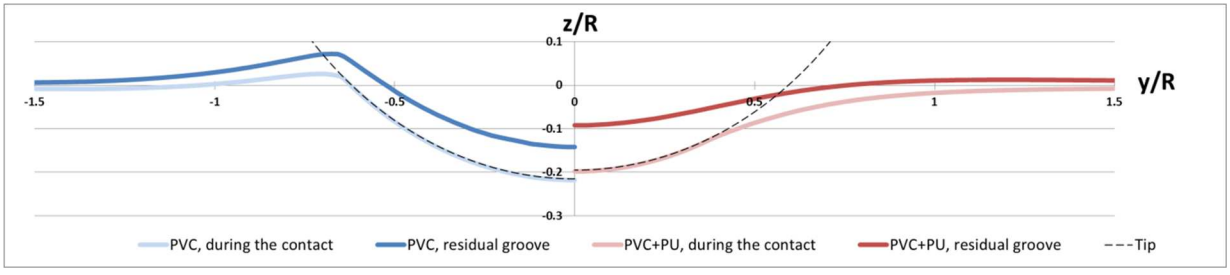

Figure 7: cross-sections of the grooves during the contact and after the elastic springback for: uncoated PVC (left) and coated PVC (right)

- **Uncoated PVC**: The penetration depth is 0.22R. During the contact, the material fits the shape of the tip. Moreover, there is a pile up (lateral bulge) on the side of the contact with a well-defined ridge at the edge of the contact with the tip. Therefore the attack angle of the tip on the PVC is high and the contact radius between the tip and the material is high (a_c/R = 0.65). The residual depth is 0.14R, meaning an elastic unload in the bottom of the groove of 36%

- **Coated PVC**: The penetration depth is 0.2R. During the contact, there is a large sink-in effect of the material under the load. Therefore, the attack angle is less than on uncoated PVC, and contact radius is lower (a_c/R = 0.4). The residual depth is 0.09R, meaning an elastic unload in the bottom of the groove of 55% i.e. much more than for uncoated PVC.

From these two simulations, the plastic dissipation power is computed as a function of the displacement of the tip. It corresponds to the total power spent to deform the material plastically, as illustrated by eq.4. The curves are plotted figure 9.

$$P_{pl} = \int_V \overline{\sigma}_{eq} \,.\, \dot{\overline{\varepsilon}}_{pl} \qquad (4)$$

With V the volume of the domain, $\overline{\sigma}_{eq}$ the equivalent stress and $\dot{\overline{\varepsilon}}_{pl}$ the equivalent plastic strain rate.

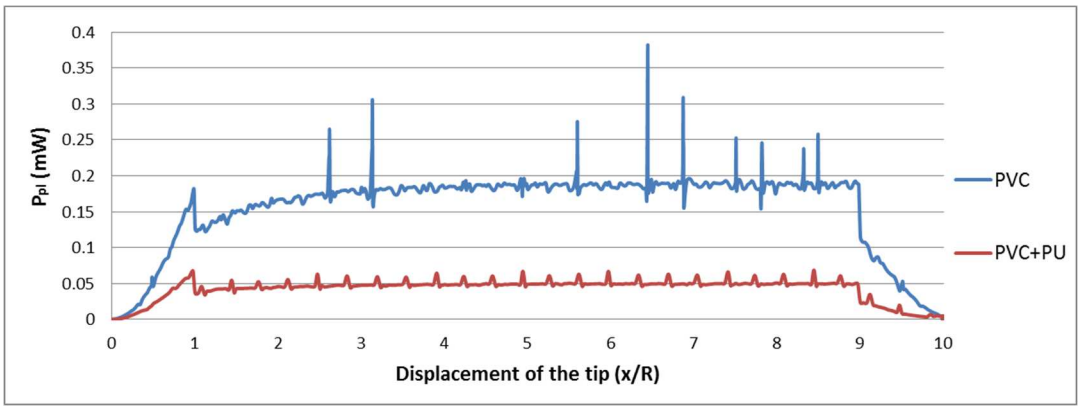

Figure 8: Plastic dissipation power in function of the tip displacement, for uncoated and coated PVC. Peaks are numerical artefacts corresponding to mechanical field transport after remeshing.

In the stationary regime, the uncoated PVC dissipates 0.2 mW plastically while the coated PVC dissipates 0.05 mW. In other words, uncoated PVC plastifies much more than coated PVC during a scratch test, for a same normal load applied on the tip.

3.2.3 Analysis of the three rupture mechanisms

Two numerical simulations have been carried out:

1) The first simulation is done with a vertical tip displacement of d = 0.4 R (i.e. twice the thickness of the coating). This vertical displacement leads to a normal force of Fn = 1.14N. This corresponds to part 4 of figure 2.

2) The second simulation is done with a tip vertical displacement of d = 0.5 R (2.5 x coating thickness). This vertical displacement leads to a normal force of Fn = 1.7N. This corresponds to part 5 of figure 2.

The results of the two computations are presented in figure 10. The color code gives the intensity of the first (highest, most tensile) principal stress, whereas grey arrows indicate the corresponding principal direction.

- d = 0.4 R: There are two different locations of stress concentration.
  The first one is at the top surface of the coating, at the rear side of the contact edge. The principal axis is oriented at ≈ 45° to the scratch direction.
  The second stress concentration is under the tip, in the symmetry plane y = 0, at the coating/substrate interface. This stress is oriented along the axe (Oy).
- d = 0.5 R shows three stress concentration:
  The previous two are still present, but their values have significantly increased. The main difference is the formation of a frontal bulge. Because of this bulge, the coating is solicited in bending in front of the tip so there is a large tensile stress on the top of the bulge (external surface of the coating), forming a circle ahead of the front of the contact. This stress is oriented in the radial direction with respect to the tip centre, i.e. for example the Ox direction on the (xz) symmetry plane.

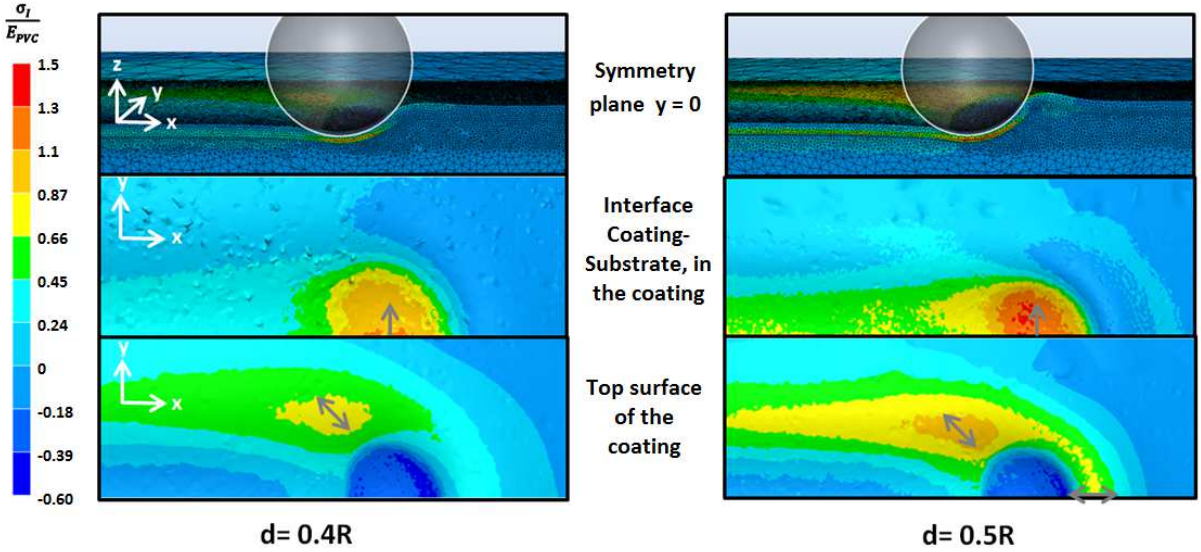

Figure 9: Numerical results: 1st principal stress normalized by the Young's modulus of the substrate. Computations done for a tip vertical displacement of d = 0.4 R (left) and d = 0.5 R (right). The grey arrows show the principal direction of the stress tensor corresponding to σ_I at the interesting areas.

Other simulations have been carried out for different vertical displacement of the tip, from d = 0.1 R to 0.6 R leading to normal forces from Fn = 0.2N to 2.1N. For each simulation The first principal stress values have been recorded at the three areas where stress concentrations are observed in figure 10: behind the tip out of the symmetry plane, under the tip at the interface, in front of the tip at the surface. The results are plotted figure 11.

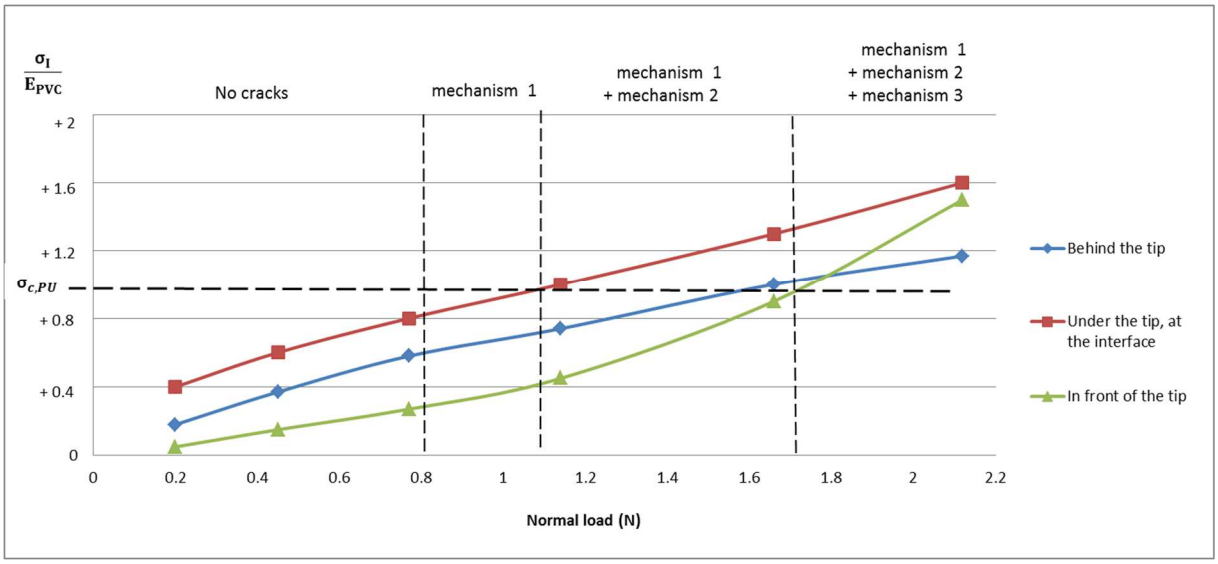

Figure 10: 1st principal stress normalized by the Young's modulus of the substrate in function of the normal load applied to the tip, in the three areas of interest (tensile stress concentrations) . The appearance of fracture mechanisms 1, 2 and 3 is positioned according to experiments.

In the three zones, the 1st principal stress is an increasing function of the normal load applied on the tip. For F_n =0.8N (the normal load at which the 1st mechanism appears experimentally), $\sigma_I = 0.6\ E_{PVC}$ behind the tip. For F_n =1.1N (the normal load at which the 2nd mechanism appears), $\sigma_I = 1\ E_{PVC}$ under the tip at the interface. For F_n = 1.7N (the normal load at which the 3rd mechanism appears) $\sigma_I = 1\ E_{PVC}$ in front of the tip. This gives us a first approach of the coating toughness in terms of critical stresses.

4. Discussions

4.1 Influence of the coating on the geometry of the contact and on plastic strain

When the thickness of the coating is negligible in front of the size of the scratching asperity, the coating only modifies friction and/or envelops elastically the roughness of the asperity to avoid creating micro grooves inside the macro groove (2).

On the other hand, if the thickness is very large compared with the scratching asperity size and its penetration depth, the coating behaves like a bulk and the scratch behavior is governed by the mechanical properties of the harder coating rather than those of the softer substrate.

In the case studied in this article, the size and the penetration depth of the tip is of the same order of magnitude as the coating thickness: these two interpretations of how a coating may improve scratch resistance become insufficient.

The numerical simulations of figure 8 show that in this case, for a given normal force imposed to the tip, the coating does not have a big influence on the penetration depth (the difference between the uncoated and the coated material is 0.02R). However, the elastic unloading and the plastic power dissipation are completely different: the uncoated material undergoes much more plasticity than the coated one. This difference does not result from a smaller penetration depth but from the geometry of

the contact. As shown figure 8, in the contact, due to the occurrence of pile-up in the uncoated case versus sink-in in the coated one, the slope of the furrow in the coated material is much lower.

It is admitted in the literature that the equivalent strain of a material during a scratch test can be computed for spherical tips as a function of the contact and tip radii (5) (28):

$$\varepsilon_{eq} = 0.2\frac{a_c}{R} \qquad (5)$$

In our case, $\frac{a_{c,uncoated}}{R} = 0.65$ and $\frac{a_{c,coated}}{R} = 0.4$, so $\varepsilon_{eq,uncoated} = 0.13$ and $\varepsilon_{eq,coated} = 0.08$, which explains the lower plasticity in the coated material ($\varepsilon_{yield,PVC} = 0.05$), even if the penetration depth is almost the same in the two cases.

Qualitatively, the way a hard coating increases the scratch resistance of a soft substrate, when $d \sim t_{coating}$, can be explained by the modification of the contact geometry. By increasing the global elastic deflection of the material, the coating blunts the geometry of the scratching asperity, reducing the attack angle thus the equivalent deformation of the substrate.

To achieve this objective, the coating needs to be harder than the substrate, which generally implies a more brittle behavior. PVC is ductile on a large deformation range and even at high deformation, no cracks are observed during a scratch test. The PU coating decreases the plastification of PVC, leaving shallower grooves at low load, but its brittle behavior leads to cracks at higher loads.

4.2 Cracks at 45°, behind the tip (fracture mechanism 1)

Cracks at 45° are initiated on the rear edge of the tip as shown by the in situ vision, at a distance from the symmetry plane ; starting from the side of the contact, they propagate outward. However, in-situ optical observation cannot tell where, in the depth, these cracks are initiated. The numerical simulations show a localization of tension on the rear face of the tip, away from the symmetry plane, precisely at the location where these cracks are initiated experimentally. Moreover, at this place, the 1st principal stress is oriented at ~ 45° (perpendicular to the crack propagation direction), which explains this fracture mode. This concentration of stress is localized on the top surface of the material, meaning that the crack is initiated on the extreme surface and then propagates along the direction –z down to the interface, together with the x+y direction.

4.3 Tearing under the tip (fracture mechanism 2)

Under the tip, the flexible and ductile PVC easily deforms. The PU that adheres on it follows its deformation and is therefore solicited in bending. Because of this bending, tensile stress appears in the PU at the interface PVC/PU. The elastic-brittle PU cracks under this tensile stress. The numerical simulation shows a stress concentration in the PU under the tip near the interface. The first principal direction is (Oy) which explains the initiation of the longitudinal tearing with a recognizable crack tip in the contact area (part 4 of figure 3). Unlike the cracks at 45° that are initiated at the surface and propagate downward (in the –z direction), this tearing is initiated at the interface and propagates upward through the PU (+z direction). It also propagates in the –z direction from the interface into PVC. Indeed two scenarios may occur: either the crack propagates at the interface PU/PVC, leading to delamination of the coating, or into the bulk PVC. The tomography shows that there is no

delamination and a blunt crack propagates in the PVC instead of the interface (figure 5b), then stops at a certain depth. This observation confirms the strong adhesion between the two layers. Subsequently, the tangential displacement of the tip in the direction +x imposes that the crack spreads in the same direction. Then the crack deviates from the central axis, because of local defects (PU thickness variation, local friction coefficient variation …) that create an asymmetry in the stress field.

4.4 Cracks in front of the tip (fracture mechanism 3)

At higher deformation level, in situ observations show that the cracks at 45° and the tearing mechanism under the tip still occur. Moreover, there is a circular crack forming in front of the tip, the principal direction is radial (Ox on the symmetry plane). This crack is symmetrical with respect to the vertical plane containing the movement of the center of the tip. Again, the in situ observation does not show why, and where in the depth the crack is initiated. The answer is given by the numerical simulation which shows the formation of a frontal bulge (figure 10). On the top of this bulge, the coating is solicited in bending which leads to tensile stresses oriented in the (Ox) direction. These tensile stresses are responsible for the rupture of the coating in front of the tip. Moreover, this numerical simulation shows that the crack is initiated at the coating upper surface and propagates in the –z direction.

Since the rupture and the stress relaxation that follows is not taken into account, the numerical modelling developed does not allow ascertaining a scenario for the succession of cracking events, but a probable scenario can be proposed. After the formation of the frontal bulge, the tip climbs over this "wrinkling" and slides past it, resuming contact with uncracked coating, and the mechanism starts again after a motion of ca. two contact lengths (the length necessary to rearm the stress field). Then the three fracture mechanisms can be reset.

Again, the three mechanisms are triggered independently of each other, and it can be assumed that the stress relaxations linked to each one do not reduce the stress values far enough to prevent the apparition of the other mechanisms. This explains the coexistence of these three mechanisms.

4.5 Evaluation of a critical rupture stress of the PU

From figure 11, the stress in the PU coating that initiates each fracture mechanism may be evaluated. The second mechanism is initiated, experimentally, for a normal force of F_n = 1.1N which corresponds, in the simulation, to a stress of $1E_{PVC}$ under the tip, at the interface. The third mechanism is initiated, experimentally, for a normal force of F_n = 1.7N which corresponds, in the simulation, to a stress of $1E_{PVC}$ in front of the tip. So the mechanisms 2 and 3 (mode I) are triggered for the same value of stress $\sigma_{c,PU} \approx 1.E_{PVC}$.

The first mechanism is initiated, experimentally, for a normal force of F_n = 0.8N, which corresponds, in the simulation, to a stress of $0.6.E_{PVC}$ behind the tip, away from the symmetry plane. This stress is lower than the stress that triggers the 2nd and the 3rd mechanism. Two explanations can be proposed:

- either the first mechanism is not a mode I opening, meaning that the first principal stress is not the relevant criterion. It could be a mode II opening caused by shear stresses for exemple.

- or the value of the friction coefficient used in the numerical model is underestimated. Indeed, if the 1st mechanism is effectively a mode I opening, the stress under the tip is an increasing function of the friction coefficient (the higher the friction coefficient, the higher the tensile forces behind the tip, the higher the stress).

4.6 Applicability of the results for different values of R

In this article, all the experiments and simulations were done with a R = 100µm tip. Are these results still valid if we change the radius of the tip ?

On uncoated materials, the average deformation is independent on the scale but only depends on the ratio a_c/R (as long as all characteristic dimensions of the polymeric macromolecular structure are negligible in front of R). Therefore, the deformation regime (elastic, elastoplastic, ductile…) is independent of the scale.

On coated materials however, it is not the case. Indeed, the deformation regime depends on the ratio between R and the thickness of the coating $t_{coating}$, as explained in section 4.1: there is a structure effect. The deformation regime may be independent on R, as long as the ratio $t_{coating}/R$ is constant (0.2 in our case).

It is more difficult to conclude on fracture: cracks are initiated from defects in the material (air bubbles, bad adhesion between the particles and the matrix…), and these defects have a given density and a given size δ, independent of $t_{coating}$. Therefore, the a_c/R ratio at which the cracks are initiated probably depends on δ/R, so the cracks profile might be different depending on the scale, even for a same $t_{coating}/R$ ratio.

4.7. Influence of the fillers on the rupture initiation

The local friction is very different for the test performed on filled coating ($\mu = 0.35$) and on unfilled coating ($\mu = 0.7$), probably because the smooth unfilled PU surface results in a large adhesive friction term, contrary to the rough filled PU surface where the indenter mostly contacts mineral filler particles. Moreover, it is well known in the litterature that the mechanical response of a material during a scratch test is very sensitive to friction (27). Therefore, it is not surprising to observe some differences in the mechanical behavior with filled and unfilled coating since the friction is very different.

The three same mechanisms appear with filled and unfilled coating, which have very different local friction. Therefore, it can safely be said that these three mechanisms are the consequence of the structure of the material (rigid-brittle coating on soft elastoplastic substrate). So, the difference between the uncoated PVC and the coated one during the scratch tests comes from the structure difference, not from the difference in roughness and friction.

But the most interesting phenomenon is the difference of periodicity in the initiation of the ruptures in the two experiments (periodic for the filled coating, periodic with the same period but with missing occurrences for the unfilled one). Our interpretation is the following :

The periodicity comes from the stationary regime of the deformation. The tip deforms the material until it achieves a critical deformation which initiates a crack. The consequence of this crack is a stress relaxation which has an influence on a given length. Then, the tip keeps moving on and once it has crossed this certain distance, the material can reload and this mechanism starts again.

However, as mentioned section 4.6, a crack needs a defects to be initiated. With fillers in the coating, the volumic density of defect is high (each particle). Therefore, as soon as the stress is high enough to initiate a rupture, it is initiated directly from a particle because there is necessarily a sufficiently close one. Then, the material reloads and a new crack appears as soon as the critical stress is achieved, for the same reason : the apparition of cracks is periodic.

With unfilled coating, this reasoning does not work : as there are no fillers, the volumic density of defects is much lower. Therefore, when the critical stress is achieved, there is not necessarily a defect close enough to initiate a crack. : the apparition of cracks loses its periodicity.

5. Conclusion

In this paper, the mechanical behavior during a scratch test of soft polymer substrate coated by a harder, more brittle polymer is studied under loads such that the scratch depth is of the order of the coating thickness.

At low loads, the coating increases the scratch resistance by decreasing the plastic deformation of the substrate. However, in connection with its hardness, the coating is more brittle than the substrate and fractures at higher loads. Observations and simulations show three successive rupture mechanisms at growing load and penetration : cracks at 45° behind the tip, tearing under the tip and circular cracks in front of the tip on top of the frontal bulge. These 3 rupture mechanisms superimpose to each other rather than replacing each one, which is particularly interesting.

In situ vision shows where are initiated and how the different cracks propagate in the surface plane. Tomography, which is a real novelty in the analysis of a scratch test, gives information about the depth at which the cracks is finally present. Finally, FEM explains the mechanical conditions leading to each rupture mechanism, especially the depth at which they are initiated.

In summary, the three tools used (in situ vision + X-Ray tomography + numerical simulation) are very complementary and allow a good understanding of a complex coating damage mode involving three competing damage mechanisms observed on this bimaterial. Indeed, the successive apparition of three rupture mechanisms which don’t influence each other is a particularily interesting phenomenon whose analysis would have not been possible without the combination of these three tools.

References

1. **S.J.Bull.** Failure mode maps in the thin film scratch adhesion test. *Tribology international.* 1997, Vol. 30, 7, pp. 491-498.

2. **I.Demirci, C.Gauthier, R.Schirrer.** Mechanical analysis of the dammage of a thin polymeric coating during scratching: role of the coating thickness to the roughness of a scratching tip. *Thin solid films.* 2005, Vol. 479. pp. 207-215

3. **K.Holmerg, A.Laukkanen, H.Ronkainen, K.Wallin, S.Varjus.** Tribological contact analysis of a rigid ball sliding on a hard coated surface Part II: Material deformations, influence of coating thickness and Young's Modulus. *Surface and Coatings Technology.* 2006, Vol. 200, 12-13, pp. 3810-3823.

4. **C.Gauthier, R.Schirrer.** Time and temperature dependance of the scratch properties of poly(methylmethacrylate) surfaces. *Journal of materials science.* 2000, Vol. 35, pp. 2121-2130.

5. **C.Gauthier, S.Lafaye, R.Schirrer.** Elastic recovery of a scratch in a polymeric surface: experiments and analysis. *Tribology International.* 2001, Vol. 34, 7, pp. 469 - 479.

6. **H.Pelletier, A-L.Durier, C.Gauthier, R.Schirrer.** Viscoelastic and elastic-plastic behaviors of amorphous polymeric surfaces during scratch. *Tribology International.* 2008, Vol. 41, 11, pp. 975-984.

7. **B.J.Briscoe, P.D.Evans, S.K.Biswas, S.K.Sinha.** The hardness of poly(methylmethacrylate). *Tribology international.* 1996, Vol. 29, 2, pp. 93-104.

8. **J-L.Bucaille, C.Gauthier, E.Felder, R.Schirrer.** The influence of strain hardening of polymers on the piling up phenomenon is scratch tests: Experiments and numerical modelling. *Wear.* 2006, Vol. 260, 7-8, pp. 803-814.

9. **A.Schallamach.** How does rubber slide ? *Wear.* 1971, Vol. 17, 4, pp. 301-312.

10. **V.Jardet, P.Morel.** Viscoelastic effects on the scratch resistance of polymers: relationship between mechanical properties and scratch properties at various temperatures. *Progress in organic coatings.* 2003, Vol. 48, 2-4, pp. 322-331.

11. **M.C. Baietto, J. Rannou, A. Gravouil, H. Pelletier, C. Gauthier, R. Schirrer.** 3D crack network analysis during a scratch test for a polymer: A combines experimental and multirigid X-FEM based numerical approach. *Tribology International.* 2011, 44, pp. 1320-1328.

12. **B.J.Briscoe, E.Pelillo, S.K.Sinha.** Scratching hardness and deformation maps for polycarbonate and polyethylene. *Polymer engineering and science.* 1996, Vol. 36, 24, pp. 2996-3005.

13. **P.J.Burnett, D.S.Rickerby.** The relationship between hardness and scratch adhesion. *Thin solid films.* 1987, Vol. 154, 1-2, pp. 403-416.

14. **V.Le Houerou, C.Robert, C.Gauthier,R.Schirrer.** Mechanical analysis of blistering and chipping of a scratch-resistant coating. *Wear.* 2008, Vol. 265, 3-4, pp. 507-515.

15. **V.Le Houerou, C.Gauthier,R.Schirrer.** Mechanical analysis of the blistering of a thin film deposited on a glassy polymer. *Tribology international.* 2010, Vol. 43, 1-2, pp. 129-135.

16. **J-L.Bucaille.** *Simulation numérique de l'indentation et de la rayure de verres organiques.* PhD dissertation, Ecole nationale supérieure des mines de paris, 2001.

17. **J-L.Bucaille, E.Felder, G.Hochstetter.** Mechanical analysis of the scratch test on elastic and perfectly plastic materials with the three dimensional finite element modeling. *Wear.* 2001, Vol. 249, 5-6, pp. 422-432.

18. **K.L.Johnson.** The correlation of indentation experiments. *Journal of the Mechanics and Physics of Solids.* 1970, Vol. 18, 2, pp. 115-126.

19. **J.Goddard, H.Wilman.** A theory of friction and wear during the abrasion of metals. *Wear.* 1962, Vol. 5, 2, pp. 114-135.

20. **K.Holmerg, A.Laukkanen, H.Ronkainen, K.Wallin, S.Varjus, J.Koskinen.** Tribological contact analysis of a rigid ball sliding on a hard coated surface Part I: Modelling stresses and strains. *Surface and Coatings Technology.* 2006, Vol. 200, 12-13, pp. 3793-3809.

21. **A.Laukkanen, K.Holmerg, J.Koskinen, H.Ronkainen, K.Wallin, S.Varjus.** Tribological contact analysis of a rigid ball sliding on a hard coated surface Part III: Fracture toughness calculation and influence of residual stresses. *Surface and Coatings Technology.* 2006, Vol. 200, 12-13, pp. 3824-3844.

22. **J.LI, W.Beres.** Three dimensional finite element modelling of the scratch test for a TiN coated titanium alloy substrate. *Wear.* 2006, Vol. 260, 11-12, pp. 1232-1242.

23. **G.Kermouche, N.Aleksy, J.L.Loubet, J.M.Bergheau.** Finite element modeling of the scratch response of a coated time-dependent solid. *Wear.* 2009, Vol. 267, 11, pp. 1945-1953.

24. **H.Jiang, R.Browning, J.D.Whitcomb, M.Ito, M.Shimouse, T.A.Chang, H-J.Sue.** Mechanical Modeling of scratch behavior of polymeric coatings on hard and soft substrates. *Tribology Letters.* 2010, Vol. 37, 2, pp. 159-167.

25. **M.Hamdi, X.Zhang, H-J.Sue.** Fundamental understanding on scratch behavior of polymeric laminates. *Wear.* 2017, Vols. 380-381, 15, pp. 203-216.

26. **M.M.Hossain, S.Xiao, H-J.Sue, M.Kotaki.** Scratch behavior of multilayer polymeric coating systems. *Material & design.* 2017, Vol. 128, 15, pp. 143-149.

27. **S.Lafaye, C.Gauthier, R.Schirrer.** A surface flow model of scratching tip: apparent and true local friction coefficients. *Tribology international.* 2005, Vol. 38, 2, pp. 113-127.

28. **D.Tabor.** *The Hardness of metals.* 1951. Oxford University Press.

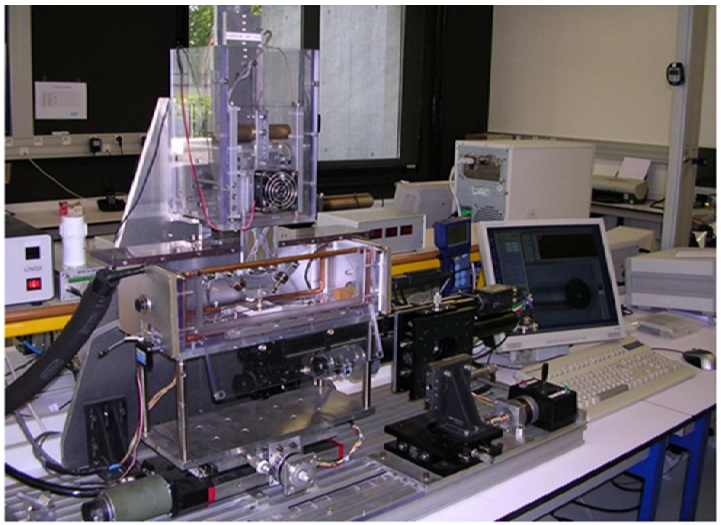

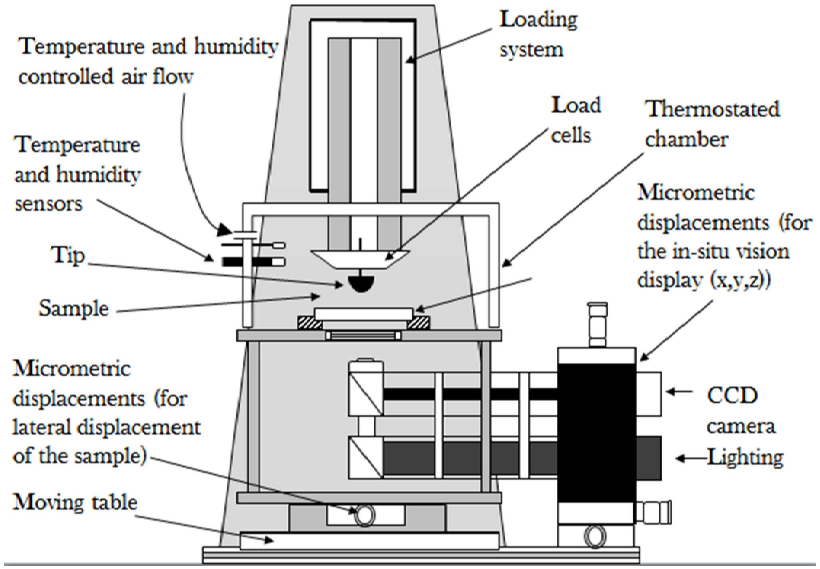

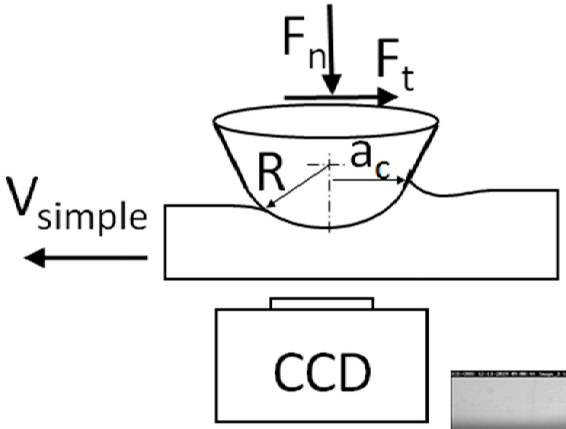

Example of a scratch on a transparent and smooth polymer: PMMA, increasing normal load from 0.25 to 4 N (time two for each level), R=100µm, RT, V = 30µm/s, image size 512µm by 384 µm.

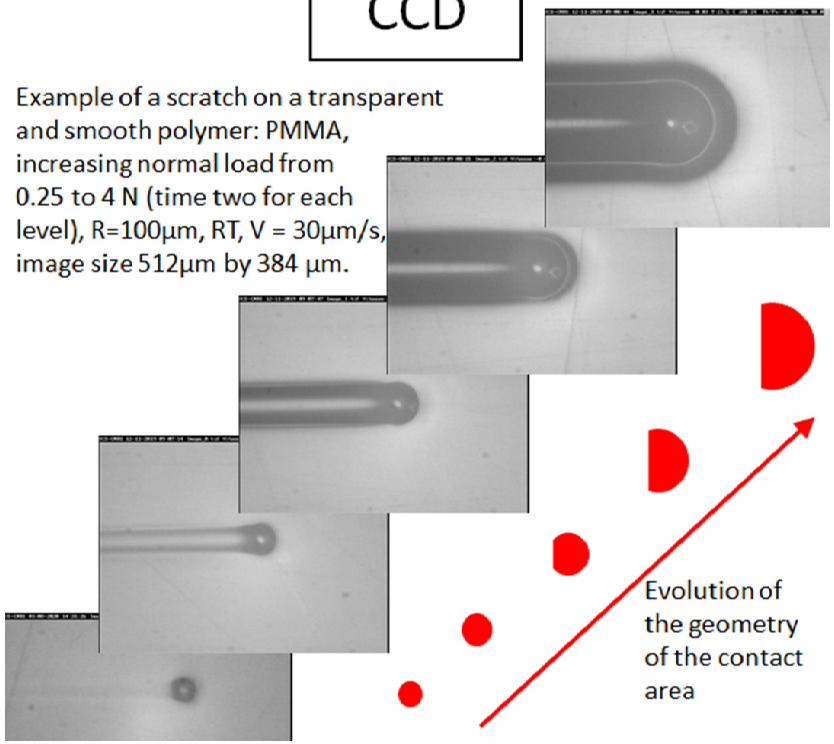

Appendix A

Appendix B

The next scan was performed with the following parameters: Resolution = 1.4 µm, RX energy = 80 kV, 11550 projections carried out over 8 rotations, in helical mode with a vertical displacement of the sample. Averaging = 10 images per position. The sensor has a cadence of 3 images per second. The whole scan lasts 10.7 hours. The reconstruction method used is the filtered back projection Size of the scan: 8.4 mm x 1.3 mm x 0.9 mm

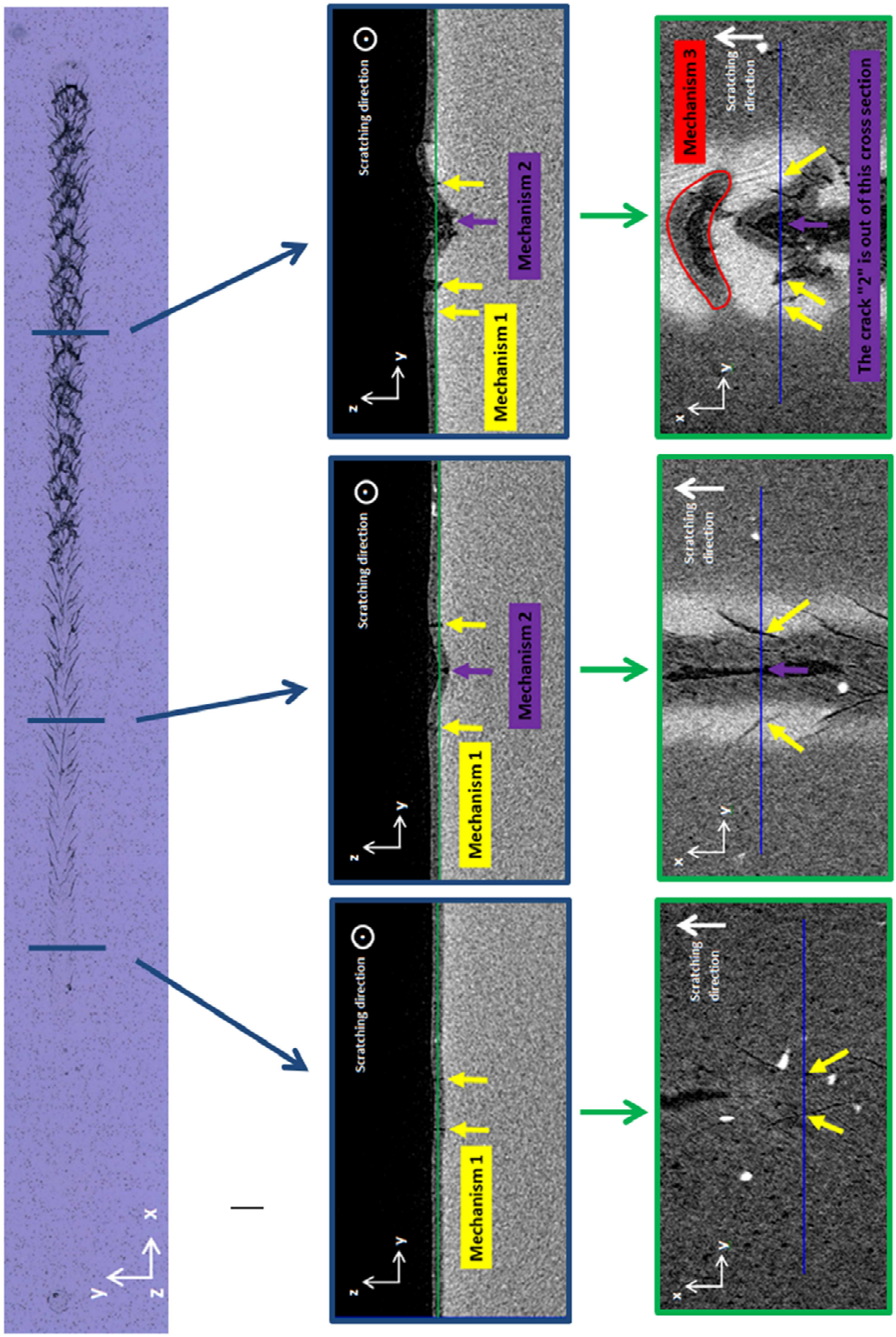

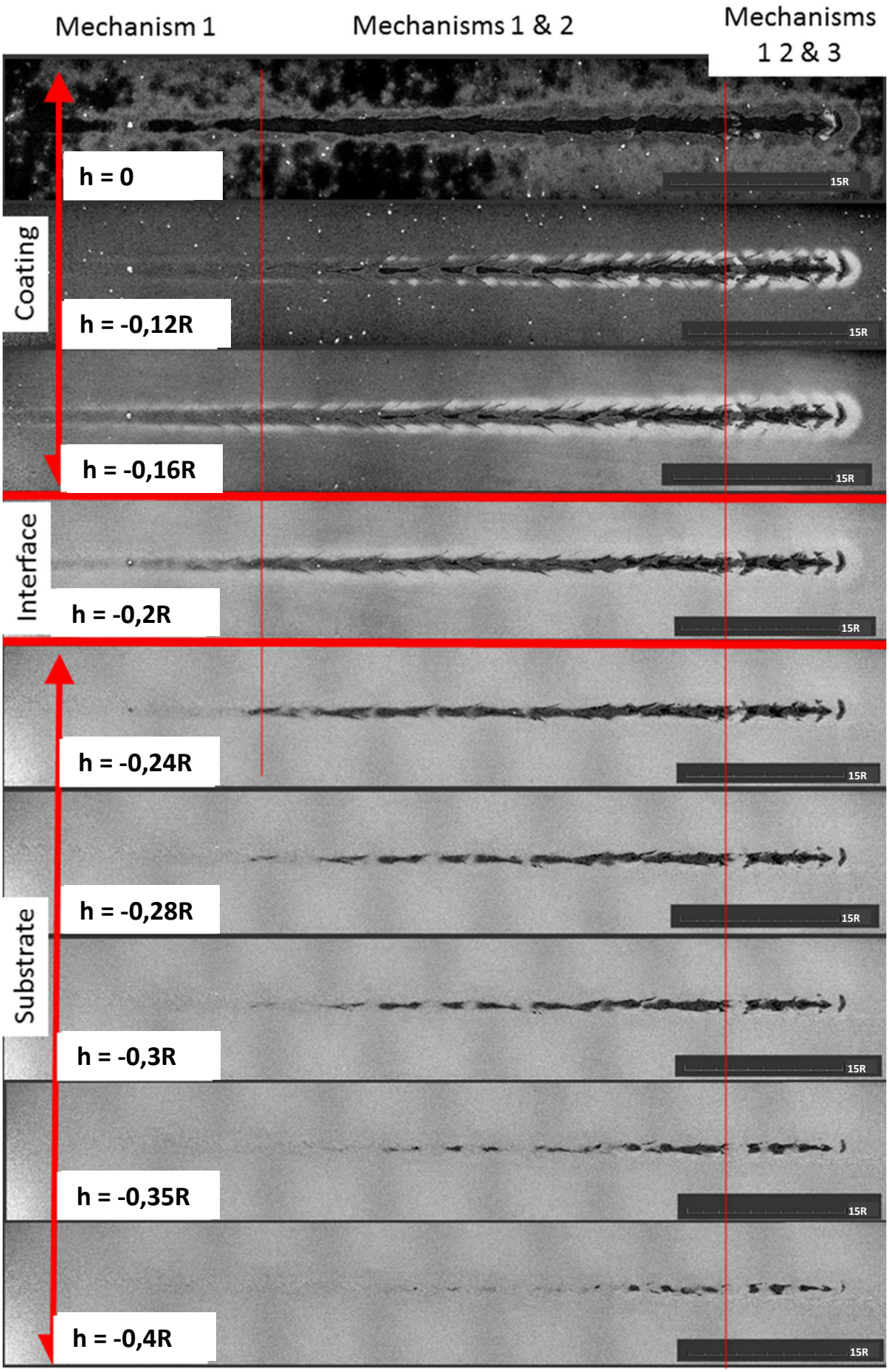
Mechanism 1
Mechanisms 1 & 2
Mechanisms 1 2 & 3
Coating
Interface
Substrate
h = 0
h = -0,12R
h = -0,16R
h = -0,2R
h = -0,24R
h = -0,28R
h = -0,3R
h = -0,35R
h = -0,4R
15R